J. Fluid Mech. (2013), *vol.* 732, *pp.* 29–46. © Cambridge University Press 2013
doi:10.1017/jfm.2013.384

Scaling laws for the thrust production of flexible pitching panels

Peter A. Dewey[1],†, Birgitt M. Boschitsch[1], Keith W. Moored[2], Howard A. Stone[1] and Alexander J. Smits[1,3]

[1]Department of Mechanical and Aerospace Engineering, Princeton University, Princeton, NJ 08544, USA
[2]Department of Mechanical Engineering and Mechanics, Lehigh University, Bethlehem, PA 18015, USA
[3]Monash University, Clayton, VIC 3800, Australia

(Received 27 March 2013; revised 17 July 2013; accepted 21 July 2013)

We present experimental results on the role of flexibility and aspect ratio in bio-inspired aquatic propulsion. Direct thrust and power measurements are used to determine the propulsive efficiency of flexible panels undergoing a leading-edge pitching motion. We find that flexible panels can give a significant amplification of thrust production of $\mathcal{O}(100\text{–}200\,\%)$ and propulsive efficiency of $\mathcal{O}(100\,\%)$ when compared to rigid panels. The data highlight that the global maximum in propulsive efficiency across a range of panel flexibilities is achieved when two conditions are simultaneously satisfied: (i) the oscillation of the panel yields a Strouhal number in the optimal range ($0.25 < St < 0.35$) predicted by Triantafyllou, Triantafyllou & Grosenbaugh (*J. Fluid Struct.*, vol. 7, 1993, pp. 205–224); and (ii) this frequency of motion is tuned to the structural resonant frequency of the panel. In addition, new scaling laws for the thrust production and power input to the fluid are derived for the rigid and flexible panels. It is found that the dominant forces are the characteristic elastic force and the characteristic fluid force. In the flexible regime the data scale using the characteristic elastic force and in the rigid limit the data scale using the characteristic fluid force.

Key words: biological fluid dynamics, propulsion, swimming/flying

1. Introduction

Animals often propel themselves through a fluid by employing flexible appendages that generate lift and thrust forces while producing highly three-dimensional wakes (Lauder *et al.* 2011). It was hypothesized, and later confirmed, that there is considerable advantage in using flexible propulsors instead of rigid ones that depend on the kinematics of the motion, the planform shape and structural stiffness (Katz & Weihs 1978; Heathcote, Wang & Gursul 2008; Michelin & Smith 2009; Eldredge, Toomey & Medina 2010; Masoud & Alexeev 2010; Kang *et al.* 2011; Ramananarivo, Godoy-Diana & Thiria 2011; Dai *et al.* 2012). Gains of over 100 % in net thrust (Ramananarivo *et al.* 2011) and propulsive efficiencies (Dai *et al.* 2012) have been observed, primarily due to improved hydrodynamic factors associated with the bending of the surface (Ramananarivo *et al.* 2011; Dewey, Carriou & Smits 2012), as well

† Email address for correspondence: pdewey1@gmail.com

as to the exploitation of the structural resonances of flexible structures (Masoud & Alexeev 2010).

Although Kang *et al.* (2011) noted that it is now generally accepted that operating near a structural resonant frequency will result in an enhanced thrust performance, the exact role that resonance plays in enhancing efficient performance remains unclear. For example, certain insects oscillate their wings well below their natural resonant frequency (Sunada 2002), and a number of studies of flapping flight have observed that flexible wings display a peak efficiency at frequencies between one-third and one-half of the resonant frequency. In this respect, Vanella *et al.* (2009) numerically investigated a two-dimensional two-link structure and suggested that animals oscillate well below their primary structural resonance, measured in a vacuum, in order to capture the benefits of a superharmonic nonlinear resonance at one-third of the primary resonance. Ramananarivo *et al.* (2011) offered that in bending a flexible wing can take on a more aerodynamically efficient shape that becomes optimal at 70 % of the resonant frequency. Using an order of magnitude scaling argument, Kang *et al.* (2011) predicted that optimal efficiency occurs at 40 % of the resonant frequency. In contrast, for a heaving flexible wing in the two-dimensional inviscid limit, Michelin & Smith (2009) found a peak in efficiency at a particular structural resonance frequency, and for a flexible wing at a net angle of attack, Masoud & Alexeev (2010) observed an efficiency maximum at 1.2 times the resonant frequency. The limited data on the role of structural resonance in water also suggest that optimal conditions occur very near a resonant frequency (Spagnolie *et al.* 2010; Moored *et al.* 2011; Alben *et al.* 2012; Leftwich *et al.* 2012).

Another question that needs further attention is the coupling between flexibility and three-dimensional effects. Many investigations have considered two-dimensional flow past flexible oscillating structures in both the inviscid (Katz & Weihs 1978; Michelin & Smith 2009; Alben *et al.* 2012) and viscous regimes (Vanella *et al.* 2009; Eldredge *et al.* 2010). A number of studies have also examined the flow past three-dimensional flexible oscillating structures (Masoud & Alexeev 2010; Moored *et al.* 2011; Ramananarivo *et al.* 2011; Dai *et al.* 2012; Leftwich *et al.* 2012), although in these particular investigations the geometry of the propulsive surface was fixed and only the stiffness was varied. Dai *et al.* (2012) suggested that the effects of aspect ratio in the rigid case (examined by Buchholz & Smits (2008)) can be extrapolated to the flexible case, but this has not yet been verified.

Motivated by these observations, we perform experiments on the behaviour of rectangular flat plates undergoing a pitching motion at a moderate Reynolds number ($Re = 7200$). First, we investigate the coupling between aspect ratio and stiffness of the propulsive surface. Second, we examine the role of structural resonance in generating unsteady propulsion. The kinematic motion (leading-edge pitching) and rectangular planform were selected for their simplicity so that the effects of flexibility and aspect ratio could be isolated. The considerable amount of previous work on similar pitching panels by, for example, Buchholz & Smits (2008), Green & Smits (2008) and Dai *et al.* (2012) also helps to provide a context for this work. We report measurements of the thrust production, power input to the fluid and propulsive efficiency for a range of input oscillation frequencies, aspect ratios and panel stiffnesses. We propose an argument to explain the role of structural resonance in generating efficient propulsion, and develop new scaling laws that collapse the data for flexible as well as rigid panels.

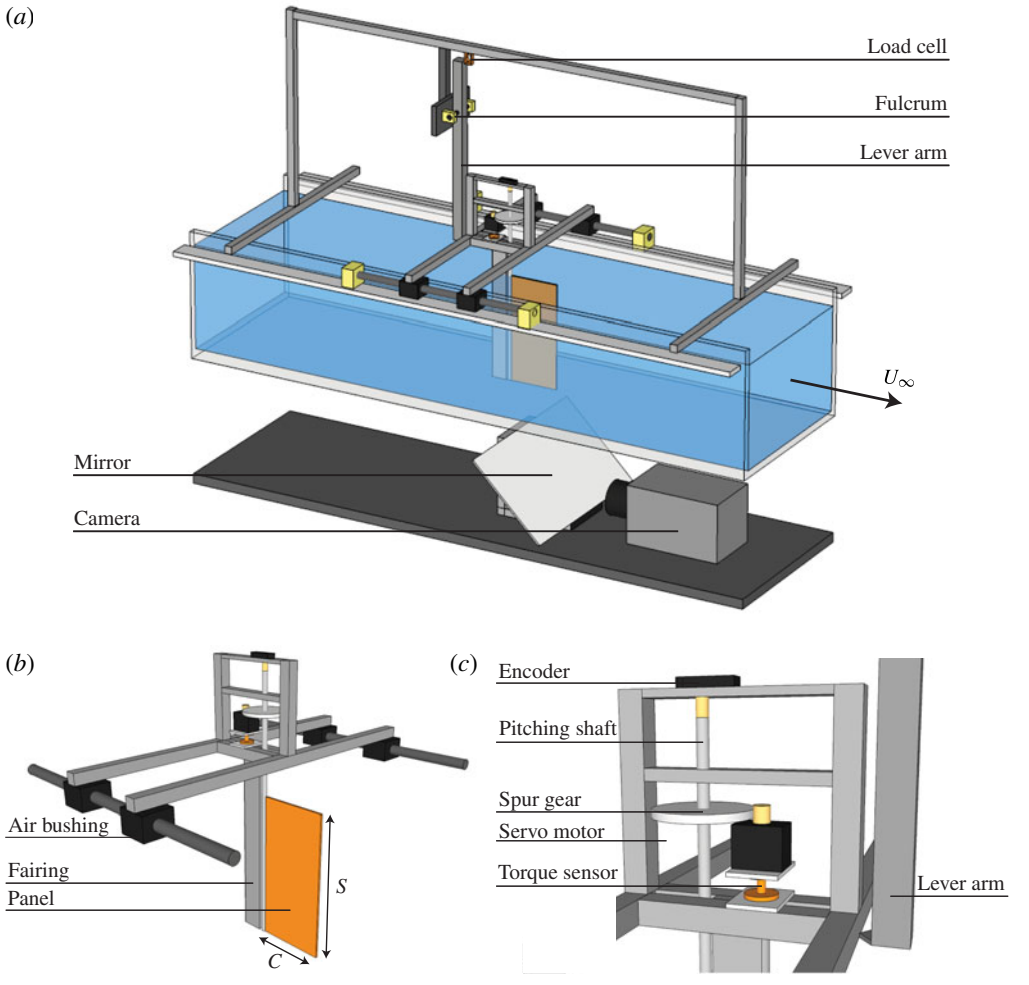

FIGURE 1. (Colour online) Experimental set-up. (*a*) Perspective view of the entire set-up. Note that the load cell and support for lever arm are rigidly mounted to an external support that is fixed in the laboratory. (*b*) Detailed view of the pitching panel rig, note that the chord length C and span length S of the panel are defined here. (*c*) Detailed view of the actuation mechanism.

2. Experimental set-up

Experiments were conducted in a closed-loop, free-surface water channel with a test section 0.46 m wide, 0.3 m deep and 2.44 m long. The experimental apparatus is shown in figure 1. The free stream velocity, $U_\infty = 0.06$ m s^{-1}, was selected to achieve a Reynolds number based on the panel chord length ($C = 120$ mm) of $7200 \pm 3\,\%$ so that direct comparisons to Buchholz & Smits (2008) could be made. The leading edge of the panels was attached to a pitching shaft located just downstream of a NACA 0012-64 stationary fairing (chord length of 50.8 mm but truncated at two-thirds of the chord) that suppressed leading-edge vortex formation. Note that the panel chord length defined here refers to the chord length of the panel itself and does not include the chord length of the stationary fairing. An acrylic sheet spanning the width of the channel was used to suppress the free-surface disturbances caused by the oscillating

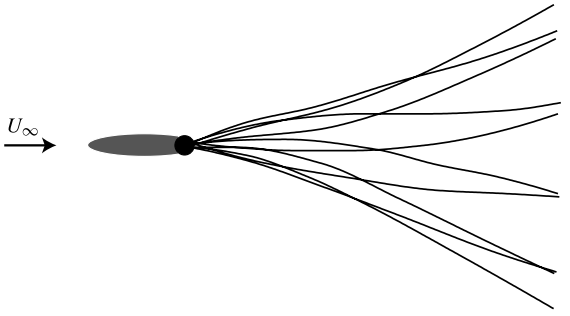

FIGURE 2. Characteristic kinematics of a flexible pitching panel at resonance at 10 time points in its oscillation period. Note that the leading-edge fairing remains stationary throughout the oscillation period. Kinematics shown are for panel P_4 at $k = 9.1$ and $\mathcal{AR} = 0.5$.

panel. The sheet was in contact with the surface of the water and extended 0.75 m downstream and 0.3 m upstream of the leading edge of the fairing.

The pitching shaft was oscillated at a frequency f using a servo motor coupled to the shaft via a spur gear with a 5:1 ratio. The motion was verified by coupling a US Digital S1 optical encoder directly to the shaft to measure the oscillations. Altogether, 27 evenly spaced frequencies, corresponding to reduced frequencies from $k = 2\pi fC/U_\infty = 2.3$–$18.8$, were examined for each panel. For all cases considered here, the maximum pitching angle of the leading edge, $\theta_0 = 0.25$ rad, was held constant and chosen such that the peak-to-peak amplitude of motion of the trailing edge of the rigid panel was $A_\infty = 0.25C$. The peak-to-peak amplitude of motion, A, is defined as the lateral excursion of the trailing edge of the panel at its midspan. In all cases, the measured pitching angle varied by less than 1 % and the frequency varied by less than 0.1 % from the input values. The amplitude of motion and kinematics of the flexible panels depend on the passive response of the panel, as discussed below. The shape of a typical flexible pitching panel at various points in the flapping cycle is shown in figure 2.

The panel actuation mechanism was mounted on a low-friction air-track system using cylindrical air bushings aligned with the flow direction. The mechanism abutted against a lever arm and the air bushing system was forward biased by angling the tracks by 0.5° to ensure that the apparatus was always in contact with the lever arm since the actuation mechanism was not rigidly attached to the lever arm. The net thrust (or drag) produced by the panel was determined by subtracting the forward bias force from the total force measured by the Omega LCAE-600 load cell. The dynamics of the lever arm system are described by Buchholz, Clark & Smits (2008). Note that the flow velocity is imposed on the panel so that a positive net thrust indicates that the channel flow speed is slower than the speed that would be achieved by the freely swimming panel.

The average power required to actuate the panel, $\mathscr{P}_a$, was found by measuring the reaction torque, τ, on the motor using an Omega TQ-202 torque sensor, and the angular velocity, $\dot{\theta}$, by using an optical encoder ($\mathscr{P}_a = T_p^{-1} \int_0^{T_P} \tau \dot{\theta}\, \mathrm{d}t$). The power required to overcome the mechanical friction in the system, $\mathscr{P}_f$, was found by actuating the system with the panel removed. The power delivered to the fluid is then $\mathscr{P} = \mathscr{P}_a - \mathscr{P}_f$. The variances in the average value of the thrust and power were <7 % and <15 %, respectively.

Panel	P_1	P_2	P_3	P_4	P_5	P_6	P_∞
Π_1	0.3	0.7	1.4	2.0	4.0	7.8	$\mathcal{O}(10^4)$
$h/C(\times 10^{-3})$	1.1	1.6	2.1	3.2	4.2	5.3	26.5

TABLE 1. Physical properties of the panels.

The chord length for all of the panels was fixed at 120 mm, and the aspect ratio of the panels, $\mathcal{R} = S/C$, was varied by changing the span S. The flexibility of the panel is described by the effective stiffness of the panel Π_1, defined by

$$\Pi_1 = \frac{Eh^3}{12(1-\nu_p^2)\rho_f U_\infty^2 C^3}, \tag{2.1}$$

where E is the elastic modulus of the material, $h^* = h/C$ is the non-dimensional panel thickness, ν_p is Poisson's ratio for the panels and ρ_f is the fluid density (Kang *et al.* 2011). The panels were made from polyethylene plastic with a density $\rho_s = 1300$ kg m^{-3}, that is, a specific gravity $\rho^* = \rho_s/\rho_f = 1.3$. Seven panels with different flexibilities were considered, including one rigid panel (see table 1). The flexibilities of the panels were selected such that the flexural stiffness (EI, where I is the area moment of inertia) ranged from 4.2×10^{-4} to 1.1×10^{-2} Nm^2, covering the range of flexural stiffnesses seen in biological propulsors (Lauder *et al.* 2011). The panels will be referred to as P_1–P_6 for the flexible panels, where subscripts 1–6 indicate the range from the most to the least flexible panel, with P_∞ denoting the rigid panel.

Two sets of experiments were conducted so that the parameters of interest, aspect ratio and flexibility, could be systematically isolated from one another. In the first set, all seven flexibilities were considered and the panels spanned the entire depth of the water channel ($\mathcal{R} = 2.4$) to generate a nominally two-dimensional flow field. In the second set, only panels P_4, P_5 and P_∞ were considered and four different aspect ratios were considered ($\mathcal{R}$= 0.5, 1.0, 1.5, and 2.0).

The peak-to-peak amplitude of motion of the trailing edge of the flexible panels, A, is an output from the system that depends on the balance between inertial, elastic and external fluid forces (Daniel & Combes 2002). It was measured by observing the trailing edge of the panels as they oscillated, and the results are given as a function of reduced frequency in figure 3. For all flexible panels the spanwise deflection of the trailing edge of the panel was found to be negligible. The Strouhal number, $St = fA/U_\infty$, has been used extensively in the literature; however, we prefer to present our results as a function of reduced frequency since the Strouhal number is an output of this system. We see that for panels P_3–P_6 the amplitude A reaches a maximum at a given frequency, which we denote as the resonant frequency of the first bending mode (f_1) of the panel-fluid system. Panels P_1 and P_2 do not display a maximum since for these cases the resonant frequency of the first beam bending mode is lower then the frequencies examined here. For the other panels, the maximum values of A are ∼20–30 % higher than that of the rigid panel, which agrees with the work of Dai *et al.* (2012). Also, decreasing the aspect ratio moves the peak to higher reduced frequencies, and decreasing the flexibility leads to a higher amplitude of motion. The latter observation must be limited eventually in its scope since the rigid panel by definition has a non-dimensional amplitude of unity.

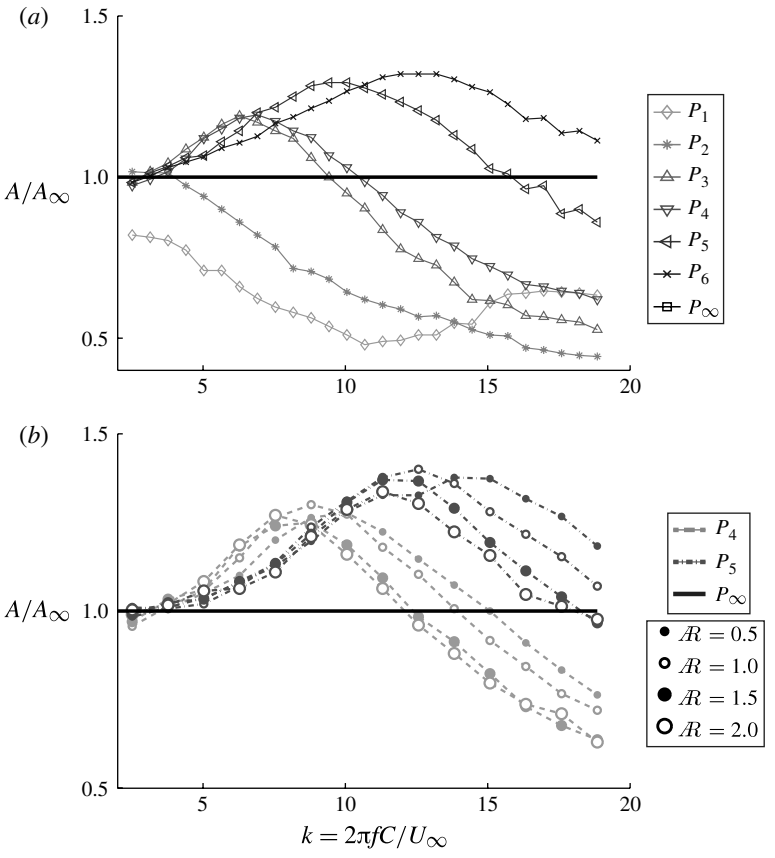

FIGURE 3. Peak-to-peak amplitude of motion of the trailing edge of the flexible panels as a function of reduced frequency. (*a*) Fixed aspect ratio panels, $\mathscr{R} = 2.4$. (*b*) Varying aspect ratio panels: P_4 dashed lines, P_5 dot-dashed lines. The amplitude is normalized by A_∞, the amplitude of motion of the rigid panel.

3. Propulsive performance results

The average net thrust (T) and average power input to the fluid ($\mathscr{P}$) are typically given in non-dimensional form by the coefficients of thrust C_T and power, C_P, where

$$C_T = \frac{T}{\frac{1}{2}\rho_f U_\infty^2 SC} \quad \text{and} \quad C_P = \frac{\mathscr{P}}{\frac{1}{2}\rho_f U_\infty^3 SC}. \tag{3.1}$$

The propulsive efficiency is then defined as the Froude efficiency given by

$$\eta = \frac{TU_\infty}{\mathscr{P}} = \frac{C_T}{C_P}, \tag{3.2}$$

To maximize the propulsive efficiency it is desirable to generate large thrust forces while expending as little power as possible.

The thrust coefficients are shown as a function of reduced frequency in figure 4. For the flexible panels, for all aspect ratios considered here, the thrust coefficient initially increases with k until a maximum is reached after which it declines slightly with a

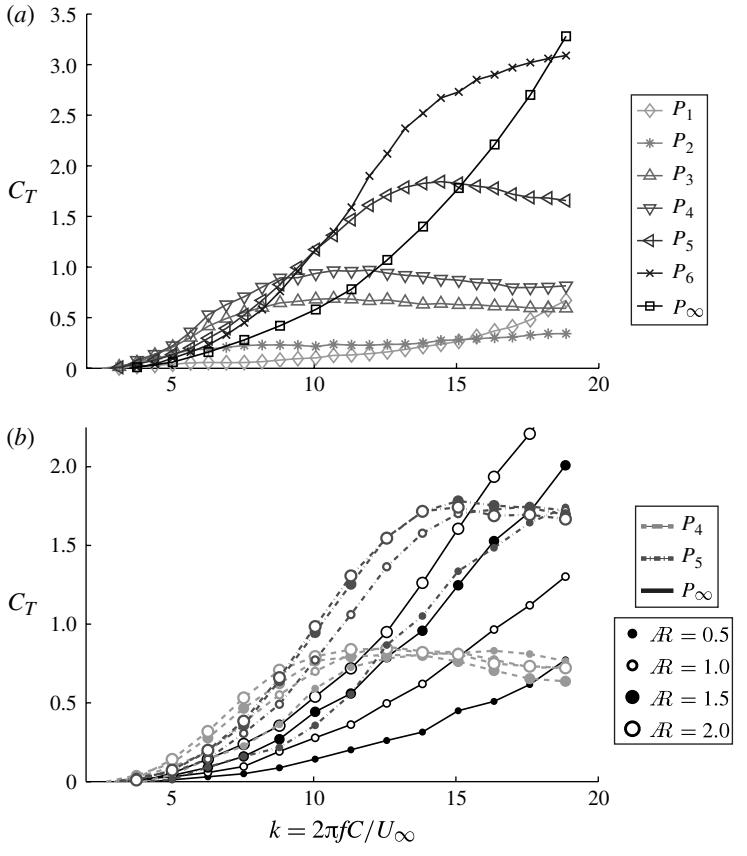

FIGURE 4. Coefficient of thrust as a function of reduced frequency for (*a*) nominally two-dimensional panels ($\mathcal{AR}$= 2.4) and (*b*) finite aspect ratio panels.

further increase in k. The peaks occur at a frequency that is ∼50 % higher than the structural resonance frequency f_1 for each panel. The structural resonant frequency of the panels is more closely aligned with the inflection point of the curves. In general, we see that the maxima in the thrust coefficients for the flexible panels increase with increasing stiffness. Buchholz & Smits (2008) and Green & Smits (2008) noted that the coefficient of thrust for a rigid panel increases with increasing aspect ratio, a result that is confirmed in the present study. In contrast, the flexible panels do not exhibit a monotonic trend with aspect ratio. Consider the data for panel P_4. At lower frequencies, the coefficient of thrust increases with aspect ratio; while at higher frequencies it decreases with aspect ratio. Thus, it is shown for the first time that with varying aspect ratio the thrust response of the panels depends on the stiffness of the panel. Intuitively, changing the aspect ratio is expected to augment the circulatory and reactionary forces imposed on the panel. In the elastic regime, this will be directly coupled to a modification of the elastic deformation of the panel. However, in the rigid limit, the panel kinematics are restricted from changing regardless of aspect ratio. So it is perhaps not surprising that there is differing behaviour in the elastic and rigid regimes when the aspect ratio is varied.

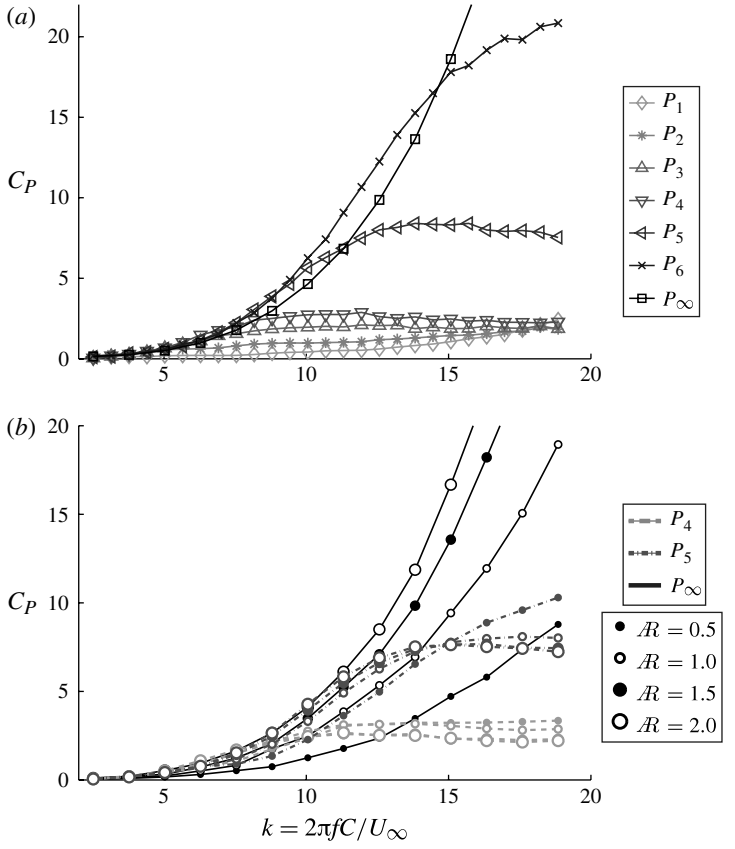

FIGURE 5. Coefficient of power as a function of reduced frequency for (*a*) nominally two-dimensional panels ($\mathcal{AR}$= 2.4), and (*b*) finite aspect ratio panels.

By comparing the flexible and rigid panels for a given aspect ratio, it can be seen that each of the flexible panels generates a higher thrust coefficient than its rigid counterpart over a certain frequency range. For example, at $k \approx 10$ with $\mathcal{AR}$= 2.4, the results in figure 4(*a*) indicate that the stiffer panels (P_5 and P_6) yield thrust coefficients that are twice as large as the rigid panel (P_∞). For the smallest aspect ratio considered, P_5 produces twice the thrust of the rigid panel while P_4 produces three times as much. With increasing frequency, the thrust coefficient produced by the rigid panel typically, but not always, outpaces that of the flexible panel because for the rigid panels the thrust coefficient monotonically increases with frequency.

The coefficient of power, C_P, is shown as a function of reduced frequency in figure 5. The results for C_P demonstrate qualitatively similar trends as those of C_T. For the rigid panels, the coefficient of power monotonically increases with reduced frequency, while for the flexible panels it initially increases with reduced frequency until a maximum is reached at which point the coefficient of power levels off. The peak in C_P occurs at a frequency that is ∼50 % higher than the structural resonance frequency, which is the same point where the thrust reached its maximum. The coefficient of power monotonically increases with aspect ratio in the rigid case, while there is no monotonic trend observed in the flexible case. This is consistent with the

thrust response of the flexible panels (figure 4) and denotes a difference between the propulsive characteristics of the rigid and flexible panels. The qualitative similarities between the trends of thrust and power, including the coincidence of the peaks in thrust and power, is attributed to the expectation that both the thrust production and power input will scale with the same characteristic force imposed on the structure. As described by Knoller (1909) and Betz (1912), the thrust production of harmonically oscillating panels is merely the component of lift in the streamwise direction. Here, lift refers to the force perpendicular to the instantaneous relative velocity. The moment, or torque, imposed on the pitching panel is the component of lift in the transverse direction times some characteristic moment arm. This implies that we should expect qualitatively similar trends in the thrust and power curves.

In the thrust response, all of the flexible panels outperformed the rigid panels over some range of frequencies. However, the coefficient of power for all flexible cases is either less than that of the rigid panel, or the relative increase in C_P is lower than the relative increase in thrust performance. This behaviour is perhaps due to the panels adopting a more aerodynamically efficient shape during their oscillation period. As noted by Ramananarivo *et al.* (2011), when a flexible panel oscillates, its trailing edge will deform with respect to the free-stream velocity. The deformed trailing edge lessens parasitic flow separation at the trailing edge, and will therefore decrease the torque (and power) required to sustain motion.

The propulsive efficiency η is given as a function of reduced frequency in figure 6. For each flexibility examined, η increases with aspect ratio as previously observed by Buchholz & Smits (2008) for rigid panels. At the highest aspect ratios, the moderately flexible panels (P_3 and P_4) yield the highest propulsive efficiencies. Either an increase or a decrease in the stiffness yields a decrease in the propulsive efficiency, indicating that there is an optimal stiffness for maximum efficiency. The global maximum efficiency for the rigid panel reaches only 16 % at $k = 6.3$, but the global maximum efficiency for the flexible panels reaches ∼38 % (panel P_3) at the same reduced frequency, a greater than 100 % increase. In addition, the flexible panels exhibit high efficiency across a wide range of frequencies whereas the rigid panels display sharper peaks. As the frequency is increased, therefore, the performance benefit of the flexible panels over the rigid panels becomes even more pronounced.

4. Role of resonance

The propulsive efficiency for the two-dimensional panels is plotted as a function of reduced resonant frequency, $f_1^* = f/f_1$, in figure 7(*a*). Here, the resonant frequency of the first beam bending mode, f_1, is determined by experiment (figure 3). The peak in propulsive efficiency for each panel is observed either below (P_5, P_6) or close to (P_3, P_4) the structural resonant frequency of the panel. The peak in propulsive efficiency for the most flexible panels, P_1 and P_2, likely occurs above the structural resonant frequency, although it was noted in figure 3 that a clear resonant frequency was not observed for these panels. From these observations, it is apparent that the resonant frequency of the structure is therefore not the primary mechanism governing efficient locomotion, and so we consider an alternative hypothesis.

Triantafyllou, Triantafyllou & Grosenbaugh (1993) performed a linear stability analysis on the two-dimensional wake of an oscillating aerofoil and found that the time-averaged wake profile was convectively unstable. They proposed that when the driving frequency of the aerofoil matched the frequency of maximum spatial growth of the instability of the velocity jet, the propulsor would maximize its work output

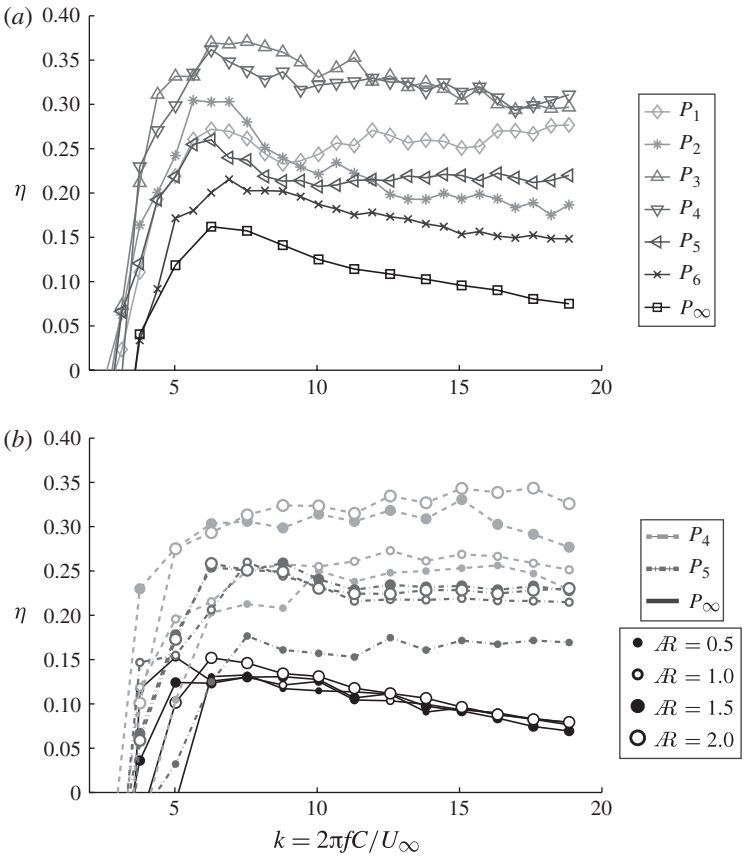

FIGURE 6. Propulsive efficiency as a function of reduced frequency for (*a*) nominally two-dimensional panels, $\mathcal{AR}$= 2.4 (*b*) finite aspect ratio panels. Symbols are the same as those used in figures 4 and 5.

for a given energy input (Triantafyllou, Techet & Hover 2004). This efficient condition was predicted to occur in a narrow Strouhal number range, $0.25 < St < 0.35$, a result supported by the observation that many animals tend to swim in this regime (Taylor, Nudds & Thomas 2003). Indeed, Lewin & Haj-Hariri (2003) and Moored *et al.* (2012) confirmed that the alignment of the driving frequency with the frequency of maximum growth of the instability (the so-called wake resonant frequency) leads to a local peak in propulsive efficiency. Moored *et al.* (2012) applied this concept to a bio-inspired propulsor that generated chordwise travelling waves, first studied by Clark & Smits (2006) and Dewey *et al.* (2012). Since the flexible panels examined in this effort generate a similar kinematic motion (figure 2), we may expect that a local peak in efficiency will be achieved when the driving frequency of the flexible panels is tuned to a wake resonant frequency.

We noted earlier that the Strouhal number for the current work is not an input parameter to the system but an output. It is interesting, therefore, that the peaks in efficiency all fall within, or very near in the case of P_1, the optimal Strouhal number range for two-dimensional propulsion predicted by Triantafyllou *et al.* (1993), $0.25 < St < 0.35$. With increasing Strouhal number the efficiency

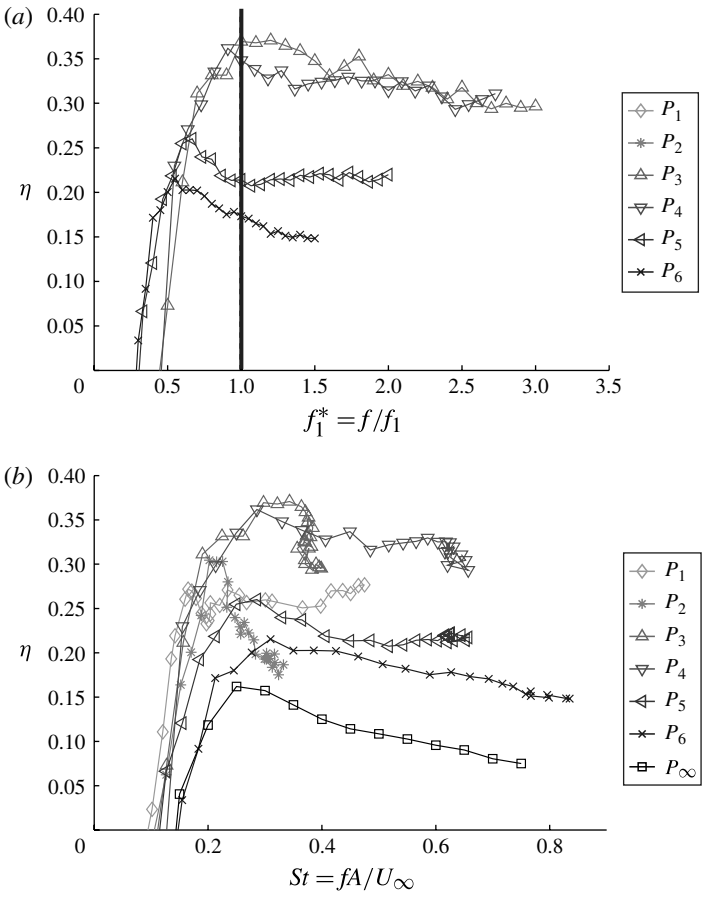

FIGURE 7. Propulsive efficiency for the nominally two-dimensional panels ($\mathcal{AR}$= 2.4) as a function of (*a*) reduced resonant frequency and (*b*) Strouhal number, $St = fA/U_\infty$.

slowly decays from the peak, but within the experimental uncertainty the efficiency is maximized within this range. It was observed that the panels that achieve the highest efficiencies (P_3 and P_4, see figure 7), are the only panels that achieve a Strouhal number within the optimal range while simultaneously operating near the structural resonant frequency. The global optimal efficiency for the two-dimensional data then occurs when two conditions are satisfied: (i) the oscillation frequency of the panel produces an amplitude of motion that yields a Strouhal number in the optimal range ($0.25 < St < 0.35$) described by Triantafyllou *et al.* (1993); and (ii) this frequency of motion is tuned to the structural resonant frequency of the panel. The first condition proposes that a local peak in efficiency will exist since it yields a Strouhal number in the optimal regime. The second condition then acts as a tuning mechanism that yields the global maximum efficiency for the two-dimensional data when the oscillation frequency is tuned to the structural resonant frequency. Since the analysis and predictions of Triantafyllou *et al.* (1993) are limited to two-dimensional flows, we hesitate to extend these conclusions to the three-dimensional case without further work.

5. Scaling

The coefficients of thrust and power, C_T and C_P, use the dynamic pressure and the planform area to make the thrust and power non-dimensional. That is, the characteristic velocity and force scales are U_∞ and $\rho_f U_\infty^2 SC$, respectively. However, when our results were presented in terms of these non-dimensional parameters, the data did not collapse. Hence, it may be interesting to consider new scaling parameters that are more suited to the performance of unsteady propulsors.

To scale the thrust and power of unsteady propulsors, consider that their dynamics will be governed by the balance between inertial, elastic, and fluid forces acting on the panel (Daniel & Combes 2002). A characteristic inertial force for the panel F_i is defined by the mass of the panel m_p $(=\rho_s SCh)$ times its characteristic acceleration (f^2C). The elastic forces depend on the flexural stiffness of the panel $(EI \propto ESh^3)$, and so a characteristic elastic force is $F_e = ESh^3/C^2$. A characteristic fluid force F_v is given by the virtual mass (m_v) times its acceleration (f^2C). In general, it is expected that the mass of fluid displaced by the panel should be the product of the fluid density, the panel area and a characteristic length that will depend on the planform shape and kinematics of the panel. For the pitching kinematics used here the amplitude of motion of the panel increases from zero at the leading edge to its maximum at the trailing edge, and so only a portion of the panel is responsible for the majority of displaced fluid. We will therefore use S^2C as the characteristic volume of displaced fluid, and the external fluid forces are then expected to scale as $F_v = \rho_f S^2 C(f^2 C)$.

Having identified these characteristic forces, we then obtain two non-dimensional parameters: Π_k, the effective stiffness of the panel given by the ratio of elastic and fluid forces; and Π_m, the effective inertia of the panel given by the ratio of the inertia and fluid forces. Hence,

$$\Pi_k = \frac{F_e}{F_v} = \left(\frac{E}{\rho_f f^2 C^2}\right)\left(\frac{1}{\mathcal{AR}}\right)\left(\frac{h^3}{C^3}\right), \tag{5.1}$$

and

$$\Pi_m = \frac{F_i}{F_v} = \left(\frac{\rho_s}{\rho_f}\right)\left(\frac{1}{\mathcal{AR}}\right)\left(\frac{h}{C}\right). \tag{5.2}$$

For thin panels oscillating in a dense fluid we expect the effective inertia of the panel to be small, indicating that the characteristic inertial forces are small in comparison with the characteristic fluid force. Under these conditions, the parameter Π_k is expected to be the more important one.

Thus far, we have used the reduced frequency $k = 2\pi fC/U_\infty$ to represent the scaling of the characteristic time, but to capture the structural response of flexible panels we turn to the unsteady Euler–Bernoulli beam equation (Allen & Smits 2001), where

$$\Pi_m \frac{\partial^2 y^*}{\partial t^{*2}} + \Pi_k \frac{\partial^4 y^*}{\partial x^{*4}} = F_f^*. \tag{5.3}$$

Here, y^* is the non-dimensional beam deflection due to bending, x^* is the non-dimensional coordinate along the length of the beam, t^* is the non-dimensional time, and F_f^* is the external force imposed on the structure normalized by F_v. We see that the effective inertia and effective stiffness parameters Π_m and Π_k identified through physical arguments arise naturally in this non-dimensional form of the equation, a similar form of which was shown by Alben (2008) and Alben (2010). Though in these works a two-dimensional treatment was considered that did not include the effect

of aspect ratio. The equation highlights that the structural resonance frequency is proportional to the ratio of the effective stiffness and the effective mass. That is,

$$\omega_n^{*2} = \beta_n^4 \frac{\Pi_k}{\Pi_m} \propto \left(\frac{f_n}{f}\right)^2, \tag{5.4}$$

where β_n represents the eigenvalue and f_n is the natural frequency corresponding to the nth eigenmode of the beam (Timoshenko 1974). Therefore, we propose that the appropriate scaling for the oscillation frequency f will relate to the structural resonant frequency of the panel (in the presence of flow), which is similar to the argument made by Thiria & Godoy-Diana (2010). For our purposes, we present this as the reduced natural frequency $f_n^* = f/f_n$ $(=1/\omega_n^*)$. In our experiments only the first bending mode was observed so that we use only f_1^*, where f_1 is determined from the results shown in figure 3.

When flexibility becomes the dominant effect (Π_k is small), as may be the case for some of the flexible panels described here, the thrust production and power input to the fluid should be scaled using the characteristic elastic force, F_e. The characteristic power expended in bending is then expressed by the product of F_e and the characteristic velocity fC. The non-dimensional thrust production and power input for flexible panels are then

$$\widetilde{C_T} = \frac{TC^2}{Eh^3S} \quad \text{and} \quad \widetilde{C_P} = \frac{\mathscr{P}C^2}{Eh^3S(fC)}. \tag{5.5}$$

In addition, a new efficiency $\widetilde{\eta}$ can be defined by considering the ratio of the new thrust parameter to the new power parameter, so that

$$\widetilde{\eta} = \frac{\widetilde{C_T}}{\widetilde{C_P}} = \frac{T(fC)}{\mathscr{P}}. \tag{5.6}$$

We see that $\widetilde{\eta}$ is similar to the Froude efficiency η given by (3.2); however, $\widetilde{\eta}$ uses fC as the characteristic velocity rather than the free stream velocity.

The thrust, power and efficiency data in this new scaling are shown in figure 8 for the flexible panel data. We observe that this scaling collapses the data remarkably well across all aspect ratios examined. Note that only the data for panels P_3–P_6 are displayed as they are the only panels that clearly display a first resonant mode. The new efficiency parameter, $\widetilde{\eta}$, monotonically increases with frequency and does not reach a maximum. This behaviour is likely due to the characteristic velocity in $\widetilde{\eta}$ being proportional to frequency, and it does not necessarily indicate that the strategy to optimize propulsive efficiency, typically defined by the Froude efficiency η, is to oscillate at high frequencies.

The scaling parameters of the thrust production and power input to the fluid show no particular dependence on the Reynolds number. For a given kinematic motion, the scaling is expected to be independent of Reynolds number. However, a variation in Reynolds number will modify the skin friction and form drag acting on the panel as it oscillates. This could alter the kinematics of the flexible panels, which would change the fluid forces acting on the panels as well as the resonant frequency of the panel. It is expected, therefore, that the effect of Reynolds number is to modify the achieved kinematics of the flexible panels, which, in turn, will modify the thrust production and power input to the fluid. This consideration merits additional study that we leave to future endeavors.

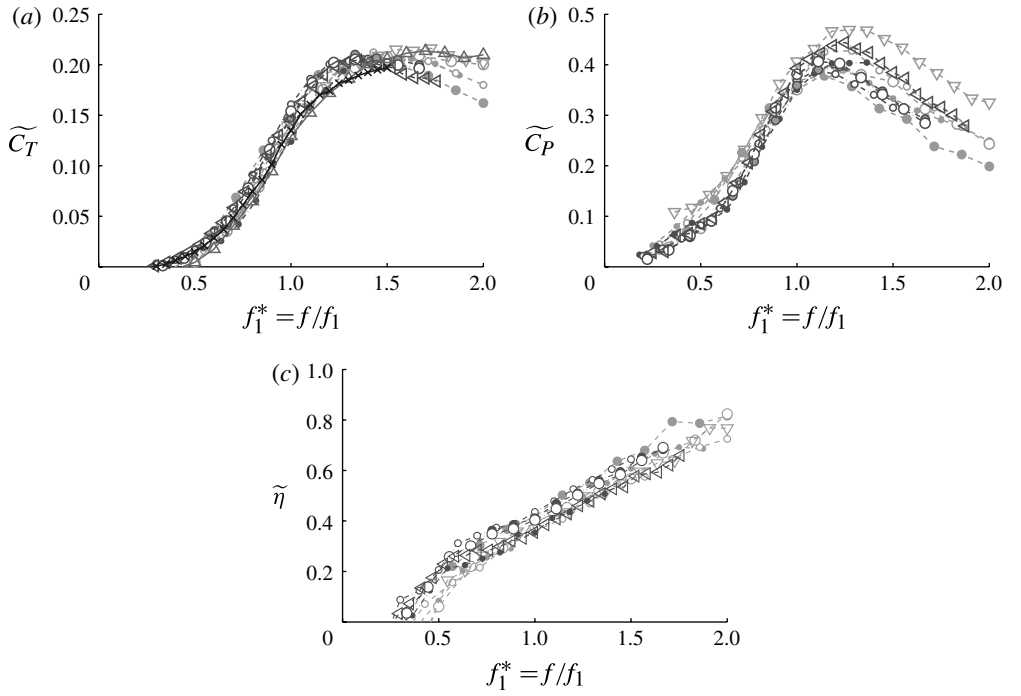

FIGURE 8. (*a*) Scaled thrust behaviour, (*b*) scaled power behaviour and (*c*) scaled efficiency behaviour. Symbols are the same as used in figures 4–7, only the flexible panel data for panels P_3–P_6 is presented here.

We now consider the behaviour of rigid panels, which is the limit where Π_k is large. Instead of scaling the thrust and power with the characteristic elastic force, which is expected to be less important in this regime, we now use the characteristic fluid force $F_v = (\rho_f S^2 C)(f^2 C)$. The non-dimensional thrust and power for rigid panels are then

$$\widetilde{T} = \frac{T}{\rho_f S^2 C (f^2 C)} \quad \text{and} \quad \widetilde{P} = \frac{\mathscr{P}}{\rho_f S^2 C (f^2 C)(fC)}. \tag{5.7}$$

The scaled efficiency for the rigid panels remains unchanged from the flexible panel scaling, which is defined in (5.6). In addition, the resonant frequency of the rigid panels is much higher than the frequencies of oscillation considered here, so that the reduced frequency k should be the correct non-dimensional frequency parameter for rigid panels, instead of f_1^*. Figure 9 shows that the data for the rigid panels collapse very satisfactorily using this representation for the thrust, power and efficiency.

Green & Smits (2008) found that the thrust produced by a rigid pitching panel is related to the unsteady lift generated by the oscillating panel and the thrust decreased with aspect ratio because of the increasing influence of the finite span. The interpretations of the current effort and that by Green & Smits (2008) may, in fact, be related. Theodorsen (1935) notes that the forces generated by harmonically oscillating plates can be decomposed into circulatory and non-circulatory components. The non-circulatory forces are related to the virtual mass term, which depend on aspect ratio, while the circulatory forces depend on the circulation distribution, and so

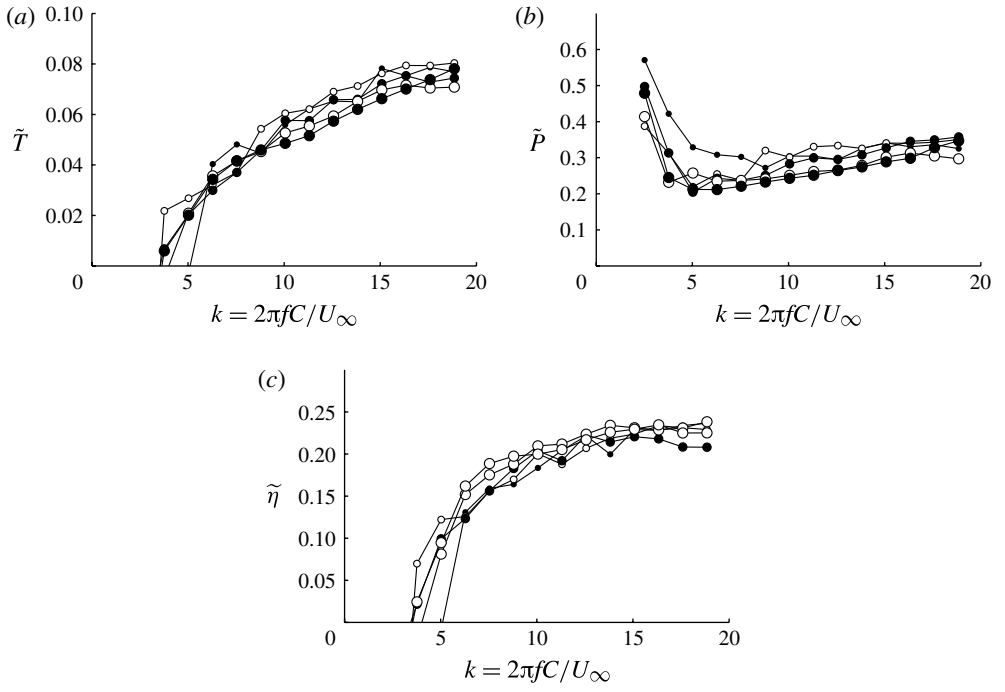

FIGURE 9. Rigid panel scaled data for (*a*) thrust, (*b*) power and (*c*) efficiency.

also depend on aspect ratio. Hence, it seems reasonable that the forces generated by the oscillating panel can be related to either the virtual mass term or the unsteady lift.

The scaling analysis presented here indicates that when the effective inertia of the panel is very small ($\Pi_m \ll 1$), the dominant forces are the characteristic elastic force and the characteristic fluid force. In the flexible regime the data scale using the characteristic elastic force and in the rigid limit the data scale using the characteristic fluid force. In general, we expect that a continuum exists between these regimes and the appropriate scaling force will be a balance of the elastic and virtual mass force. To better understand this continuum, consider that if the inertial effects of the panel can be neglected we could statically relate the non-dimensional bending deformation of the panel, δ, by considering the applied fluid forces and the flexural stiffness of the panel, $F_v = (EI/C^2)(\delta/C) = F_e(\delta/C)$. As the bending deformation becomes of a similar order to that of the chord length, the characteristic fluid force approaches the characteristic elastic force. This is expected to occur as the panels become more flexible and might relate to the transition between the regimes. Deciphering the exact nature of this continuum is difficult though based on the current investigation since the stiffness of the rigid and flexible panels differs by $\mathcal{O}(10^3)$. This difficulty could be overcome in future work by considering stiffnesses separated by evenly spaced intervals extending from the rigid to the flexible regimes.

6. Concluding remarks

In general, each flexible panel exhibited a frequency band over which it produced more thrust than a rigid panel with the same aspect ratio. The response of power

input to the fluid depends on frequency, aspect ratio and flexibility (it can increase or decrease in comparison with the rigid panel); but its rate of change is always less than the relative change in thrust, which therefore leads to a net increase in propulsive efficiency as compared with the rigid panel. It was found that the effective stiffness is important in optimizing efficiency, and when the panel is too stiff or too flexible a degradation in performance occurs. Nevertheless, the effects of flexibility on propulsion are clearly beneficial. For instance, a global maximum efficiency of $\sim$38 % was found for a moderately flexible panel, which is a greater than 100 % increase over the maximum observed for the rigid panels. By incorporating flexibility into a simple pitching mechanism there is a profound impact on propulsive efficiency, suggesting that further benefits may accrue with optimization of the actuation strategy.

Previous studies have found efficiency peaks below the resonant frequency (Ramananarivo *et al.* 2011), at the resonant frequency (Michelin & Smith 2009) and above the resonant frequency (Masoud & Alexeev 2010). In the current effort all of these cases were observed. This suggest that operating at resonance is not a sufficient condition to ensure efficient locomotion of flexible propulsors. Instead, we note that a local peak in efficiency for the two-dimensional flexible panels is observed when the panels are oscillated at a frequency that yields a Strouhal number in the optimal range ($0.25 < St < 0.35$) predicted by the two-dimensional Triantafyllou *et al.* (1993). The global maximum efficiency, at least for this data set, is then achieved in the two-dimensional case by tuning the frequency to the structural resonant frequency while still operating in the optimal Strouhal range. These observations help us to better understand the previous results presented in the literature and suggest that applying a linear stability analysis to the wakes of flexible pitching panels would prove beneficial in uncovering the physical mechanisms leading to the observed optimal flexibility.

The propulsive characteristics of both rigid and flexible pitching panels of finite aspect ratio are described well by considering the unsteady characteristics that naturally arise for harmonically oscillating panels. Our results suggest that there are two different stiffness regimes for the range of oscillation frequencies and structural stiffnesses examined here. In the rigid limit ($\Pi_k > 10^4$), the appropriate characteristic force relates to the acceleration of the virtual mass and the time scale is given by the unsteady time scale $1/f$. When the stiffness is decreased ($1 < \Pi_k < 10$) the elastic forces become more important and the appropriate characteristic force is that due to elastic forces and the time scale is given by the structural resonant frequency. Between these regimes a continuum is likely to exist that is expected to be captured by the parameter Π_k, which represents the relative importance of the characteristic elastic and fluid forces. Our conclusions are limited to cases where only the first beam bending mode was excited, but we anticipate that for highly flexible panels ($\Pi_k \ll 1$), higher-order beam bending modes will be excited. This possible regime is a subject for future work. Future efforts focused on determining the scaling of the structural resonant frequency of the flexible panels would also prove beneficial because here they were determined experimentally.

Acknowledgement

This work was supported by the Office of Naval Research under Program Director Dr R. Brizzolara, MURI grant number N00014-08-1-0642.

REFERENCES

ALBEN, S. 2008 Optimal flexibility of a flexible appendage in an inviscid fluid. *J. Fluid Mech.* **614**, 355–380.

ALBEN, S. 2010 Passive and active bodies in vortex streets. *J. Fluid Mech.* **642**, 95–125.

ALBEN, S., WITT, C., BAKER, T. V., ANDERSON, E. & LAUDER, G. V. 2012 Dynamics of freely swimming flexible foils. *Phys. Fluids* **24**, 051901.

ALLEN, J. J. & SMITS, A. J. 2001 Energy harvesting eel. *J. Fluid Struct.* **15**, 629–640.

BETZ, A. 1912 Ein beitrag zur erklaerung des segelfluges. *Z. Flugtech. Motorluftsch.* **3**, 269–270.

BUCHHOLZ, J. H. J., CLARK, R. P. & SMITS, A. J. 2008 Thrust performance of unsteady propulsors using a novel measurement system, and corresponding wake patterns. *Exp. Fluids* **45**, 461–472.

BUCHHOLZ, J. H. J. & SMITS, A. J. 2008 The wake structure and thrust performance of a rigid low-aspect-ratio pitching panel. *J. Fluid Mech.* **603**, 331–365.

CLARK, R. P. & SMITS, A. J. 2006 Thrust production and wake structure of a batoid-inspired oscillating fin. *J. Fluid Mech.* **562**, 415–429.

DAI, H., LUO, H., DE SOUSA, P. J. S. A. FERREIRA & DOYLE, J. F. 2012 Thrust performance of a flexible low-aspect-ratio pitching panel. *Phys. Fluids* **24**, 101903.

DANIEL, T. L. & COMBES, S. A. 2002 Flexible wings and fins: bending by inertial or fluid-dynamic forces. *Integr. Compar. Biol.* **42**, 1044–1049.

DEWEY, P. A., CARRIOU, A. & SMITS, A. J. 2012 On the relationship between efficiency and wake structure of a batoid-inspired oscillating fin. *J. Fluid Mech.* **691**, 245–266.

ELDREDGE, J. F., TOOMEY, J. & MEDINA, A. 2010 On the roles of chord-wise flexibility in a flapping wing with hovering kinematics. *J. Fluid Mech.* **659**, 94–115.

GREEN, M. A. & SMITS, A. J. 2008 Effects of three-dimensionality on thrust production by a pitching panel. *J. Fluid Mech.* **615**, 211–220.

HEATHCOTE, S., WANG, Z. & GURSUL, I. 2008 Effect of spanwise flexibility on flapping wing propulsion. *J. Fluid Struct.* **24**, 183–199.

KANG, C. K., AONO, H., CESNIK, C. E. S. & SHYY, W. 2011 Effects of flexibility on the aerodynamic performance of flapping wings. *J. Fluid Mech.* **689**, 32–74.

KATZ, J. & WEIHS, D. 1978 Hydrodynamic propulsion by large amplitude oscillation of an aerofoil with chordwise flexibility. *J. Fluid Mech.* **88**, 485–497.

KNOLLER, R. 1909 Die gesetze des luftwiderstandes. *Flug Motortech.* **3** (21), 1–7.

LAUDER, G. V., MADDEN, P. G. A, TANGORRA, J. L., ANDERSON, E. & BAKER, T. V. 2011 Bioinspiration from fish for smart material design and function. *Smart Mater. Struct.* **20**, 1–13.

LEFTWICH, M. C., TYTELL, E. D., COHEN, A. H. & SMITS, A. J. 2012 Wake structures behind a swimming robotic lamprey with a passively flexible tail. *J. Exp. Biol.* **215**, 416–425.

LEWIN, G. C. & HAJ-HARIRI, H. 2003 Modelling thrust generation of a two-dimensional heaving aerofoil in a viscous flow. *J. Fluid Mech.* **492**, 339–362.

MASOUD, H. & ALEXEEV, A. 2010 Resonance of flexible flapping wings at low Reynolds number. *Phys. Rev.* E **81**, 1–5.

MICHELIN, S. & SMITH, S. G LLEWELLYN 2009 Resonance and propulsion performance of a heaving flexible wing. *Phys. Fluids* **21**, 1–15.

MOORED, K. W., DEWEY, P. A., HAJ-HARIRI, H. & SMITS, A. J. 2012 Hydrodynamic wake resonance as an underlying principle of efficient unsteady propulsion. *J. Fluid Mech.* **708**, 329–348.

MOORED, K. W., DEWEY, P. A., LEFTWICH, M. C., BART-SMITH, H. & SMITS, A. J. 2011 Bioinspired propulsion mechanisms based on manta ray locomotion. *Marine Technol. Soc.* **45**, 110–118.

RAMANANARIVO, S., GODOY-DIANA, R. & THIRIA, B. 2011 Rather than resonance, flapping wing flyers may play on aerodynamics to improve performance. *Proc. Natl Acad. Sci.* **108**, 5964–5969.

SPAGNOLIE, S. E., MORET, L., SHELLEY, M. & ZHANG, J. 2010 Surprising behaviours in locomotion with passive pitching. *Phys. Fluids* **22**, 1–20.

SUNADA, S. 2002 Optical measurements of the deformation motion, and generated force of the wings of a moth, Mythimna Separata (Walker). *JSME Intl J. Ser.* B **45**, 836–842.

TAYLOR, G. K., NUDDS, R. L. & THOMAS, A. L. R. 2003 Flying and swimming animals cruise at a Strouhal number tuned for high power efficiency. *Nature* **435**, 707–711.

THEODORSEN, T. 1935 General theory of aerodynamic instability and the mechanism of flutter. *NACA Report* 496.

THIRIA, B. & GODOY-DIANA, R. 2010 How wing compliance drives the efficiency of self-propelled flapping flyers. *Phys. Rev.* E **82**, 015303(R).

TIMOSHENKO, S. 1974 *Vibration Problems in Engineering*. John Wiley and Sons.

TRIANTAFYLLOU, M. S., TECHET, A. H. & HOVER, F. S. 2004 Review of experimental work in biomimetic foils. *IEEE J. Ocean. Engng* **29**, 585–594.

TRIANTAFYLLOU, G. S., TRIANTAFYLLOU, M. S. & GROSENBAUGH, M. A. 1993 Optimal thrust development in oscillating foils with application to fish propulsion. *J. Fluid Struct.* **7**, 205–224.

VANELLA, M., FITZGERALD, T., PREIDIKMAN, S., BALARAS, E. & BALACHANDRAN, B. 2009 Influence of flexibility on the aerodynamic performance of a hovering wing. *J. Exp. Biol.* **212**, 95–105.